





ARTICLE OPEN



Identification of genes supporting cold resistance of mammalian cells: lessons from a hibernator

Masamitsu Sone^{1,2}, Nonoka Mitsuhashi^{1,2}, Yuki Sugiura^{3,4}, Yuta Matsuoka³, Rae Maeda³, Akari Yamauchi^{1,2}, Ryoto Okahashi^{1,2}, Junpei Yamashita², Kanako Sone², Sachiyo Enju², Daisuke Anegawa² and Yoshifumi Yamaguchi^{1,2,5}

© The Author(s) 2024

Susceptibility of human cells to cold stress restricts the use of therapeutic hypothermia and long-term preservation of organs at low temperatures. In contrast, cells of mammalian hibernators possess remarkable cold resistance, but little is known about the molecular mechanisms underlying this phenomenon. In this study, we conducted a gain-of-function screening of genes that confer cold resistance to cold-vulnerable human cells using a cDNA library constructed from the Syrian hamster, a mammalian hibernator, and identified Gpx4 as a potent suppressor of cold-induced cell death. Additionally, genetic deletion of or pharmacological inhibition of Gpx4 revealed that Gpx4 is necessary for suppressing lipid peroxidation specifically under cold in hamster cell lines. Genetic disruption of other ferroptosis-suppressing pathways, namely biopterin synthesis and mitochondrial or plasma membrane CoQ reduction pathways, also accelerated cold-induced cell death under Gpx4 dysfunction. Collectively, ferroptosis-suppressing pathways protect the cells of a mammalian hibernator from cold-induced cell death and the augmentation of these pathways renders cold resistance to cells of non-hibernators, including humans.

Cell Death and Disease (2024)15:685; <https://doi.org/10.1038/s41419-024-07059-w>

INTRODUCTION

Prolonged and severe low body temperature (T_b) is fatal to the majority of mammals. An exception to this rule is mammalian hibernation. Hibernation is an adaptive strategy to survive food-scarce seasons by lowering metabolism, thereby exhibiting extremely low body temperature (T_b) and saving energy expenditure [1]. During the hibernation period, small mammalian hibernators (hereafter simply termed as “hibernators”) repeat many cycles of deep torpor and periodic arousal; in deep torpor, they cease motion and largely reduce heat production and their core T_b for several days to a couple of weeks; in periodic arousal, they recover their T_b to euthermia and sustain normal activity for less than one day [2]. During deep torpor, their T_b drops to below 10 °C and becomes stable at approximately 1 °C above ambient temperature [3]. Such very low T_b causes severe cellular and organ injuries in non-hibernators, including humans, mice, and rats, but not in small hibernators [4]. However, it remains largely unknown how hibernators avoid cellular and organ injuries induced by very low T_b.

We previously reported that a hibernator, the Syrian hamster, *Mesocricetus auratus* (hereafter referred to as hamsters), is resistant to cold-induced ferroptosis in a nutrient-dependent manner [5]. Primary hepatocytes derived from hamsters fed a diet containing a high amount of α -Tocopherol (α T) exhibit cold resistance by storing high amounts of α T in the cells, whereas those from hamsters fed a low- α T diet do not [5]. In addition, primary

hepatocytes isolated from mice fed a high- α T diet fail to store high amounts of α T and do not exhibit cold resistance [5]. Thus, there is a difference in the mechanisms that exert α T-dependent cold resistance between hibernators and non-hibernators. Likewise, there is a difference in intrinsic, nutrient-independent, and cellular cold resistance between hibernators and non-hibernators. It has long been known that hibernators’ cells can survive longer than those from non-hibernators in cold temperatures lower than 10 °C, and this was recently confirmed in cell lines derived from some hibernator species [6–9]. However, little is known about the molecular mechanisms that support the cell-intrinsic cold resistance of hibernators.

Prolonged cold stress induces cell death in cells derived from non-hibernators including humans. Such cold-induced cell death fulfills the hallmarks of ferroptosis [10]. Ferroptosis is a type of regulated cell death that accompanies ferrous-ion-mediated accumulation of lipid peroxide radical [11, 12]. Along with normal cellular activities, lipid radicals are continuously produced by the oxidation of polyunsaturated fatty acids in the plasma membrane and are further oxidized into lipid peroxide radicals by molecular oxygen [13]. Lipid peroxide radicals attack adjacent lipids to produce lipid radicals and lipid peroxide, and radical-trapping antioxidants (RTA) such as α T and CoQH₂ can prevent this reaction [14–16]. Depending on the ferrous ion, accumulated lipid peroxide is converted into lipid peroxide radicals, which propagate in the cell membrane and finally induce necrotic cell death [13].

¹Graduate School of Environmental Sciences, Hokkaido University, Sapporo, Japan. ²Institute of Low Temperature Science, Hokkaido University, Sapporo, Japan. ³Multomics Platform, Center for Cancer Immunotherapy and Immunobiology, Kyoto University Graduate School of Medicine, Kyoto, Japan. ⁴Human Biology Microbiome Quantum Research Center (WPI-Bio2Q), Keio University School of Medicine, Tokyo, Japan. ⁵Inamori Research Institute for Science, Kyoto, Japan. ✉email: msone@lowtem.hokudai.ac.jp; bunbun@lowtem.hokudai.ac.jp
Edited by Mauro Piacentini

Received: 9 January 2024 Revised: 3 September 2024 Accepted: 5 September 2024

Published online: 19 September 2024

Glutathione peroxidase (Gpx) family proteins reduce a variety of reactive oxygen species (ROS) by utilizing the reductive power of glutathione. Among eight members of Gpx genes in vertebrates, Gpx4 has unique characteristics in that it functions as monomer while many of other Gpx family members do as tetramer [17] and it has a catalytic center with more “open” structure than other Gpx proteins [18]. Because of these characteristics, Gpx4 can reduce a wide variety of ROS, especially lipid peroxide, and plays a pivotal role in suppress ferroptosis [19]. Most ferroptosis-inducing drugs developed to date directly or indirectly inhibit Gpx4’s function [19, 20]. Gpx4 is ubiquitously expressed in the cytosolic and mitochondrial forms owing to its alternative transcriptional start sites [17]. Loss of *Gpx4* in mice results in embryonic lethality (E7.5) [21], indicating that the removal of lipid peroxide by Gpx4 is essential for normal development.

Recently, multiple pathways that prevent ferroptosis in parallel with Gpx4 have been discovered: (i) the plasma membrane coenzyme Q (CoQ) reduction pathway: FSP1/Aifm2 reduces CoQ to CoQH₂ depending on NAD(P)H, thereby indirectly reducing lipid peroxide radicals at the plasma membrane [15, 16]. (ii) Biopterin pathway: Biopterin, a redox cofactor of several enzymes, can suppress the propagation of lipid peroxide radicals either directly or via αT [22]. The expression levels of GCH1, the rate-limiting enzyme of the biopterin synthesis pathway, in human cancer cell lines are well correlated with resistance to ferroptosis-inducing drugs [23]. (iii) Mitochondrial CoQ reduction pathway: DHODH is a mitochondrial enzyme that functions in the uridine synthesis pathway and indirectly reduces CoQ to CoQH₂ to suppress the peroxidation of mitochondrial membrane [24]. However, the functional contribution of these pathways, as well as Gpx4, to the intrinsic cold resistance of hibernators has not been investigated.

To elucidate the mechanisms of hibernators’ intrinsic cold resistance and to uncover potential approaches to bolster cold resistance in non-hibernators, including humans, we conducted a gain-of-function screening, in which cDNA derived from a cold-resistant hamster cell line was overexpressed in a cold-sensitive human cancer cell line to identify genes that confer cold resistance to human cells. Using a genome-editing approach and functional assays, we further examined the contribution of ferroptosis-suppressing pathways to cold resistance in mammalian cells.

MATERIALS AND METHODS

Animals and housing

Four-week-old male Syrian hamsters were purchased from the breeder (SLC, Inc., Japan), fed an MR standard diet (Nihon Nosan, Japan), housed under summer-like conditions (light: dark = 14:10 h and ambient temperature = 22–25 °C). For hibernation induction, approximately 10-week old male hamsters were transferred to and housed in a cold room under winter-like conditions (light:dark = 8:16 h and ambient temperature = 4–5 °C). Typically, hamsters start hibernation within 3 months in a cold room. When the animals were immobile and had low Tb, they were judged to have deep torpor (DT). When the animals become spontaneously active after DT, they were judged as in periodic arousal (PA). Eight-week-old female C57BL/6N mice were purchased from the breeder (SLC, Inc) and fed an MR stock diet (Nihon Nosan) and housed under summer-like conditions. Animals were sacrificed by reperfusion under anesthesia with 4% isoflurane for hepatocyte isolation, or decapitation under anesthesia for liver sampling.

Chemicals

The reagents used in this study were as follows: deferoxamine (Sigma, D9533), Ferrostatin-1 (Sigma, SML0583), idebenone (Tokyo Chemical Industry, I0848), mitoquinol (Cayman Chemical, 89950), BAPTA-AM (Tokyo Chemical Industry, T2845), RSL3 (Sigma, SML2234), BODIPY C11 (Thermo Fisher Scientific, D3861), ML210 (Cayman Chemical, 23282), BH₂ (Cayman Chemical, 81882), methotrexate (Fujifilm Wako, 139-13571), and α-Tocopherol (Tokyo Chemical Industry, T2309).

Cell culture

HapT1, HT1080, and HEK293T cells were cultured in D-MEM (High Glucose) with L-Glutamine and Phenol Red (Fujifilm Wako, 048-29763), 1× penicillin–streptomycin (Fujifilm Wako), 1× NEAA (Thermo Fisher Scientific), and 10% FBS (Nichirei, Japan). For cold culture, cells were seeded into 24-well plates (Corning or Iwaki) at 0.5–1 × 10⁵/well and incubated at 37 °C overnight. On the next day, the cells were transferred to and kept in a refrigerator set at 4 °C with culture medium supplemented with 0.1 M Hepes pH7.4 (Thermo Fisher Scientific).

Cell death assay

The amount of LDH in the supernatant was measured using the Cytotoxicity LDH Assay Kit-WST (Dojindo, Japan) following the manufacturer’s instructions. The activity of LDH in each sample was normalized to that of cells completely lysed with 1% Triton X-100. The absorbance was measured at 490 nm using Cytation5 (Agilent) after a 30-min incubation at 37 °C and adding Stop solution.

Plasmids

To generate PB-TAC-BFP, we first generated PB-TAC-ERN-BFP by Gateway recombination between pENTR-tagBFP and PB-TAC-ERN (a gift from Knut Woltjen, Addgene #80475), after which the rtTA/NeoR expression cassette was deleted by BglIII/NheI digestion, end blunting, and ligation. pT2K-EF1-rtTA-Neo was prepared using the In-Fusion HD cloning kit (Takara Bio) to recombine the rtTA/NeoR expression cassette excised by NotI/NheI from the PB-TAC-ERN and Tol2 backbone linearized by PCR, using pT2K-CAGGSv3-EGFP [25] as a template. To generate transfer plasmids of lentivirus vector for overexpression, coding sequences (CDS) of hamster Dhodh or Gch1 or N-terminally 3xFlag-tagged CDS of hamster FSP1 or sequence from the first methionine to poly-adenylation signal of cytoplasmic hs- or ma-Gpx4 were amplified using cDNA from HapT1 or HT1080 and inserted into PL-sin-EF1a-EIP (a gift from James Ellis) [26] by replacing EGFP. To generate plasmids to express Cas9 and sgRNAs to knockout hamster genes, guide RNAs were designed using CRISPRdirect (<https://crispr.dbcsl.jp/>) [27], and oligonucleotides containing the guide RNA sequences were inserted into the BbsI site of pX330 or BsmBI site of lentiCRISPR v2 (both gifts from Feng Zhang, Addgene#42230 and #52961, respectively) [28]. To generate transfer plasmids of AAV for overexpression under the liver-specific TBG promoter, CDS of EGFP or a sequence from the first methionine to poly-adenylation signal of cytoplasmic maGpx4 were inserted into pENN.AAV.TBG.N-FLAG-mSTAT5bCA.WPRE.bGH (a gift from Rhonda Kineman, Addgene #184463) by replacing the N-FLAG-mSTAT5bCA.

Expression library construction

The full-length cDNA expression library was constructed using the SMARTer RACE 5’/3’ Kit (Takara Bio, 634858) according to the manufacturer’s instructions for the In-Fusion SMARTer Directional cDNA Library Construction Kit (Takara Bio, 634933). 1 µg of total RNA extracted from HapT1 cultured at 37 °C with RNeasy Mini Kit (Qiagen) was annealed with 24 pmol 3’ In-Fusion SMARTer CDS Primer (5’-CGGGGTACGATGAGAC ACCATTTTTTTTTTTTTTTTTTTVN–3’ where N = A, C, G, or T; V = A, G, or C) in 11 µL, at 72 °C, 3 min; 42 °C, 2 min; 25 °C, 5 min, followed by first strand synthesis with template switching by adding 9 µL First-strand mix (4 µL 5xFirst-Strand Buffer, 0.5 µL 100 mM DTT, 1 µL 20 mM dNTP, 1 µL SMARTer II Oligonucleotide, 0.5 µL Rnase Inhibitor, 2 µL SMARTscribe Reverse Transcriptase) at 42 °C, 90 min; 68 °C, 10 min. cDNA was amplified in two tubes containing 50 µL PCR reaction (1 µL of first-strand cDNA, 25 µL of PrimeSTAR MAX, 24 pmol of 5’RACE Universal single primer, 24 pmol of 3’ In-Fusion SMARTer PCR Primer; 5’-CGGGGTACGATGAGACACCA–3, by 18 cycles of 98 °C, 10 s; 55 °C, 5 s; 72 °C, 90 s) followed by purification with MagExtractor (Toyobo). Linearized PB-TAC plasmid was amplified in 50 µL PCR reaction (5 ng PB-TAC-BFP, 25 µL of PrimeSTAR MAX, 10 pmol of PB-TAC_cDNA_lib_IF_F2 primer; 5’-TGATACCACTGCTTGTGTACAACTGTGATGCGCCG–3’, 10 pmol of PB-TAC-ERN_cDNA_lib_IF_R primer; 5’-TCTCATCGTACCCCGAGCTAAACGCGGCCTCGAATC–3’, by 25 cycles of 98 °C 10 s; 63 °C, 5 s; 72 °C, 40 s, followed by purification with MagExtractor. cDNA was inserted into PB-TAC plasmid in 10 µL of In-Fusion reaction (100 ng of PCR-amplified cDNA, 100 ng of linearized PB-TAC, 2 µL of 5X In-Fusion HD premix) at 50 °C, 17 min, followed by ethanol precipitation. NEB 10-beta Electrocompetent *E. coli* (New England Biolabs) was transformed with the resultant DNA of the In-Fusion reaction by GenePulserII (BioRad) at 2.0 kV, 200 Ω, 25 µF, seeded on agar plates at 5000 colonies/dish, and

harvested the next day. The PB-TAC plasmid library was extracted using the Plasmid Midi Kit (Qiagen).

Expression screening of the genes rendering cold resistance

The rtTA-expressing HT1080 cell line (HT1080 T2-ERN) was established by transfection of pT2K-EF1-rtTA-Neo and pCAGGS-T2TP, followed by G418 selection. HT1080 T2-ERN cells were seeded on two 100 mm dishes at 1×10^6 cells/dish, and the next day, which is hereafter set as day 0, transfected with a complex of 12 μ g PB-TAC plasmid library, 3 μ g pCX-IFP2 a PBase-expression vector [29], 18 μ L Lipofectamine3000 and 18 μ L P3000 reagent (Thermo Fisher Scientific) per dish. On day 1, the cells were trypsinized and seeded in 20 dishes. On day 2, 1 μ g/mL of Doxycycline (Sigma) was added until the end of the experiment. On day 3, the cells were incubated in a refrigerator set at 4 °C with culture medium supplemented with 0.1 M Hepes pH7.4 (Thermo Fisher Scientific). On day 9, the cells were incubated at 37 °C, 5% CO₂ in normal culture medium until they grew to semi-confluent cell density. The cells were treated with total three cycles of 6-day cold culture and 37 °C incubation, and lysed with 50 μ g/mL Proteinase K at 56 °C, 30 min with shaking. Genomic DNA was extracted by phenol-chloroform extraction and isopropanol precipitation. Hamster genes inserted into the genome of surviving HT1080 were amplified in 50 μ L PCR reaction (1 ng of genomic DNA, 25 μ L of PrimeSTAR MAX, 10 pmol of 5'RACE Universal single primer (5'-CAAGCAGTGGTAT-CAACGAGAGT-3'), 10 pmol of PB-TAC-ERN_cDNA_lib_IF_R primer) by 30 cycles of 98 °C, 10 s; 63 °C, 5 s; 72 °C, 90 s. The resultant DNA was separated by agarose gel electrophoresis, resulting in several bands of DNA fragments. These DNA bands were individually excised and purified with MagExtractor and sequenced with a 5'RACE Universal single primer using Sanger sequencing. To evaluate the ability of each candidate gene to render cold resistance, these DNA fragments were individually inserted into PB-TAC plasmid by In-Fusion reaction, and resultant plasmid was transfected into HT1080 T2-ERN with Lipofectamine3000, and bulk cells were used for cell death assay at 4 °C, under 1 μ g/mL of Doxycycline.

Gpx4 knockout by VIKING method

Genetic disruption of Gpx4 by VIKING was performed as previous report [30]. The principle of this method is to use drug resistance for selecting knockout cells in which a donor vector containing drug resistance gene is inserted into the target genomic loci cleaved by the gene-specific sgRNA and Cas9. In this process, the donor vector is linearized within the transfected cells by Cas9/sgRNA complex derived from a donor cleaving vector. Briefly, HapT1 cells were transfected with the donor vector (pVKG-Puro), donor cleaving vector (VKG1-gRNA-pX330), and pX330 vector expressing Gpx4-targeting sgRNA (sgGpx4) using PEI MAX (Polysciences). Transfected cells were sparsely reseeded and incubated with 2 μ g/mL puromycin (Sigma-Aldrich) for a week. The resulting colonies were manually picked and expanded without puromycin. Genetic disruption of Gpx4 was confirmed by genomic PCR using a primer set flanking the targeting site of sgGpx4.

Immunoblot

Frozen liver tissues that were crushed using a Multi-beads Shocker (Yasui Kikai, Japan) or cultured cells were dissolved in RIPA buffer containing 1 \times cComplete proteinase Inhibitor Cocktail (Roche). Protein concentration in the lysates was determined using a BCA Protein Assay Kit (Thermo Fisher Scientific). Protein samples (5–25 μ g/lane) were separated by 12.5–15% SDS-PAGE and transferred onto Immobilon-P PVDF membranes (Merck Millipore). Proteins were probed in Can Get Signal Solution1 (Toyobo) using following primary antibodies: anti-Gpx4 (1:10,000, Abcam, ab125066), anti- β -actin (1:20,000, CST, 49705), anti-FSP1 (1:10,000, Proteintech, 20886-1-AP), anti-Dhodh (1:10,000, Proteintech, 14877-1-AP), anti-Gch1(1:10,000, Proteintech, 28501-1-AP), anti-Spr (1:10,000, Proteintech, 16822-1-AP). HRP-conjugated anti-rabbit-IgG antibody (1:20,000, Jackson ImmunoResearch, 111-035-003) in Can Get Signal Solution2 (Toyobo), Immobilon Western Chemiluminescent HRP Substrate (Merck Millipore), and ImageQuant LAS4000 (GE Healthcare) were used for detection.

Lipid peroxidation detection by BODIPY C11 assay

HT1080 and HapT1 cells were seeded at a density of 2×10^4 cells/well in 96 well plates.

Next day, medium was replaced with culture medium containing 10 μ M BODIPY C11 (Thermo Fisher Scientific), and cells were incubated in 5% CO₂ at 37 °C for one hour. The cells were washed three times with prewarmed

HBSS(+) and the medium was replaced with HBSS(+) supplemented with 0.1 M HEPES pH7.4 with or without 2 μ M RSL3 or 1 μ M Ferrostatin-1. Then, the cells were incubated in a refrigerator at 4 °C and fluorescent signal of BODIPY C11 was measured everyday with ex/em = 580/590 for reduced form and ex/em = 488/510 for oxidized form using Cytation5 plate reader in a monochromator mode. Time-lapse images were taken at 4 °C in a cold room using BZ-X800 (Keyence) fluorescent microscope.

Sample preparation for metabolomic and lipidomic analysis

WT or Gpx4 KO HapT1 cells were seeded onto 100 mm dishes at 3×10^6 cells/dish. On the next day, cells for day 0 samples were washed with HBSS(+) supplemented with 0.1 M Hepes pH 7.4, collected with cell scraper, centrifuged and resulting pellets were stored at –80 °C until further use. The remaining cells were transferred to and kept in a refrigerator set at 4 °C with HBSS(+)/0.1 M Hepes. Day 1 to day 7 samples were prepared in the same way with day 0 samples.

Metabolomic analysis

Methanol (500 μ L) containing internal standards (IS: Methionine sulfone and 2-morpholinoethanesulfonic acid were used as IS for cationic and anionic metabolites, respectively) was added to the frozen cell pellets, followed by sonication and the addition of half volume of ultrapure water (LC/MS grade, Wako Pure Chemicals, Tokyo, Japan) and 0.4 volume of chloroform. The suspension was centrifuged at $15,000 \times g$ for 15 min at 4 °C. The resulting upper (aqueous) and lower (organic) layers were used for hydrophilic metabolome and lipidome analysis, respectively. For hydrophilic metabolome analysis, the aqueous layer was filtered through ultrafiltration tubes (Ultrafree MC-PLHCC, Human Metabolome Technologies, Tsuruoka, Japan), and the filtrate was dried up under nitrogen gas flow. The concentrated filtrate was dissolved in 70 μ L ultrapure water. Anionic and cationic metabolites were quantified by IC-MS and LC-MS/MS, respectively.

Anionic metabolites, including sugar phosphates, organic acids, and nucleotides, were analyzed by IC-MS. An orbitrap MS system (Q-Exactive focus, Thermo Fisher Scientific) connected to a high-performance IC system (ICS-5000+, Thermo Fisher Scientific) was used for metabolite detection. The IC system was equipped with an anion electrolytic suppressor (Dionex AERS 500; Thermo Fisher Scientific) to convert the potassium hydroxide gradient to pure water before the sample entered the MS system. Separations were performed using a Thermo Fisher Scientific Dionex IonPac AS11 -HC 4 μ m particle size column with an IC flow rate of 0.25 mL/min, supplemented with a 0.18 mL/min post-column MeOH makeup flow. Potassium gradient conditions were as follows: 1 mM to 100 mM (0–40 min), 100 mM (40–50 min), and 1 mM (50.1–60 min) at a column temperature of 30 °C. The Q-Exactive focus mass spectrometer was operated in ESI-positive-negative switching mode. Full mass scans (m/z 70–900) were performed at 70,000 resolution. The automatic gain control target was set to 3×10^6 ions with a maximum ion injection time of 100 ms. The ionization parameters of the ion source were optimized: spray voltage of 3 kV, transfer tube temperature 320 °C, S-lens level 50, heater temperature 300 °C, sheath gas 36, auxiliary gas 10.

Cationic metabolites, including amino acids and nucleosides, were quantified using a triple quadrupole mass spectrometer (LCMS-8060, Shimadzu) equipped with an electrospray ionization (ESI) ion source in positive and negative ESI, multiple reaction monitoring (MRM) mode. Samples were separated on a Discovery HS F5-3 column (2.1 mm i.d. \times 150 mm, particle size 3 μ m, Sigma-Aldrich) using mobile phase A (0.1% formic acid/water) and mobile phase B (0.1% formic acid/acetonitrile) in the ratios 100:0 (0–5 min), 75:25 (5–11 min), 65:35 (11–15 min), 5:95 (15–20 min) and 100:0 (20–25 min) with a stepwise gradient at a flow rate of 0.25 ml min⁻¹ and a column temperature of 40 °C. Chromatogram peaks obtained in compound-specific MRM channels were integrated and manually confirmed. Peak quantitation values obtained for each compound were corrected for recovery by IS and cell number.

Detection of lipid peroxidation by LC-MS

Four hundred microliters of the lower layer (organic layer) was aliquoted into a separate tube, completely dried with nitrogen gas, redissolved in 70 μ L MeOH and measured by LC-MS. For lipidomic analysis, an Orbitrap MS (Q-Exactive Focus, Thermo Fisher Scientific, San Jose, CA) connected to HPLC (Ultimate 3000 system, Thermo Fisher Scientific) was used. LC and MS conditions were as described by Ruzicka et al. [31]. Briefly, samples were injected into a Thermo Scientific Accucore C18 column (2.1 \times

150 mm, 2.6 μm); mobile phase A was 10 mM ammonium formate, 50% acetonitrile (v), 0.1% formic acid (v); mobile phase B was acetonitrile/2 mM ammonium formate and isopropyl alcohol/water, 10:88:2 (v/v/v), 0.02% formic acid (v). The gradient elution profiles were as follows: 65:35 (0 min), 40:60 (0–4 min), 15:85 (4–12 min), 0:100 (12–21 min), 0:100 (21–24 min), 65:35 (24–24.1 min), 100:0 (24.1–28 min). The Q-Exactive Focus mass spectrometer was operated in both ESI positive and negative modes. After a full mass scan (m/z 250–1100), three data-dependent MS/MS runs were performed at 70,000 and 17,500 resolution, respectively. The automatic gain control target was set to 1×10^6 ions and the maximum ion injected time was 100 ms. Source ionization parameters were as follows: spray voltage 3 kV, transfer tube temperature 285 °C, S-lens level 45, heater temperature 370 °C, sheath gas 60, auxiliary gas 20. LipidSearch software (Mitsui Information, Tokyo, Japan) with the following parameters: precursor volume tolerance = 3 ppm, product volume tolerance = 7 ppm, m-score threshold = 3.

Lentivirus vector production and infection

HEK293T cells (4.5×10^6) were seeded onto a 100 mm dish, and the next day, were transfected with a complex of 5 μg of pCMV-VSV-G (RIKEN BRC, RDB04392), 5 μg of psPAX2 (a gift from Didier Trono, Addgene #12260), 5 μg of transfer plasmid and 100 μg of PEI MAX. Three days after transfection, culture supernatant was recovered and mixed with a third volume of LentiX Concentrator (Takara Bio), incubated at 4 °C overnight, and centrifuged at $1500 \times g$ for 45 min. The resulting pellet was dissolved in PBS and stored at -80 °C.

For infection, cells were seeded on plates, and the next day, they were incubated with lentivirus in the presence of 8 $\mu\text{g}/\text{mL}$ polybrene (Nacalai Tesque) for one day. The next day, the medium was changed and supplemented with 1 $\mu\text{g}/\text{mL}$ (HT1080) or 2 $\mu\text{g}/\text{mL}$ (HapT1) of puromycin. After 2- to 3-day treatment, cells were reseeded and cultured without puromycin.

AAV vector production and infection

AAV was prepared according to a previous report with some modifications [32]. HEK293T cells were seeded onto 100 mm dishes at 4.5×10^6 /dish, and the next day, were transfected with a complex of 4 μg of pAAV2/8 (a gift from James M. Wilson, Addgene #112864), 4 μg of pHelper (Takara Bio), 4 μg of transfer plasmid and 48 μg of PEI MAX per dish. The next day, the medium was changed to DMEM without serum, and the cells were incubated for 5 days. The culture supernatant was recovered, centrifuged to remove cell debris, supplemented with a fourth volume of 40% polyethylene glycol (MW8000, Sigma)/2.5 M NaCl, and incubated on ice for more than two hours. Virus was precipitated by centrifugation at $3200 \times g$, 4 °C for 30 min, dissolved in 1 mL/dish PBS containing 2.5 mM MgCl_2 , and treated with 0.25 $\mu\text{L}/\text{mL}$ Benzonase (Sigma, E1014) at 37 °C, 30 min. The reaction was stopped by adding 1 mM EDTA. Then, 0.5 mL of saturated $(\text{NH}_4)_2\text{SO}_4$ per 1 mL of the virus solution was added and centrifuged at $9000 \times g$, RT for 5 min to remove debris. The virus solution was filtered through a 0.45 μm NEW Steradisc25 (Kurabo, Japan) and subjected to ultrafiltration with Amicon Ultra-15, 100 kDa (Merck Millipore) by centrifugation at $3200 \times g$, RT, followed by three PBS washes. Filtered and concentrated virus solution was centrifuged at 15000 rpm for 5 min to remove debris and stored at -80 °C. The virus titer was quantified using the AAVpro Titration Kit (for Real Time PCR) Ver.2 (Takara Bio) according to the manufacturer's instructions.

For infection, 8- to 12-week-old C57BL/6N female mice were intraperitoneally injected with 2.5×10^{12} vg AAV. Four weeks after infection, mice were subjected to primary hepatocyte preparation.

Primary culture of hepatocytes

Murine hepatocytes were isolated and cultured as previously described [5]. Briefly, under anesthesia with 4% isoflurane, the livers of C57BL/6N mice were perfused from the portal vein with a solution containing 1 mM EGTA in $\text{Ca}^{2+}/\text{Mg}^{2+}$ -free HBSS, followed by a solution containing 1 mg/mL collagenase and $\text{Ca}^{2+}/\text{Mg}^{2+}$ in HBSS at 37 °C. Hepatocytes were mechanically dissociated in EMEM (Sigma Aldrich, M4655) containing 10% FBS, filtered through a 100 μm cell strainer, and collected by centrifugation at $40 \times g$ for 1 min. The cells were then resuspended in medium containing Percoll (GE Healthcare), centrifuged at $60 \times g$ for 10 min, washed twice in EMEM containing 10% FBS, and finally filtered with a 40 μm cell strainer.

The basal medium for culturing hepatocytes was DMEM/F12 (Gibco 21041-025) supplemented with 5 mM HEPES pH7.4, 30 mg/L L-proline, 5 g/L BSA (Sigma A1470), 10 ng/mL EGF (Sigma E4127), 1 \times Insulin, Transferrin,

Selenium, Ethanolamine Solution (ITS-X) (Thermo Fisher Scientific), 0.1 mM dexamethasone (Fujifilm Wako), 10 mM nicotinamide (Fujifilm Wako), 1 mM L-ascorbic acid 2-phosphate (Fujifilm Wako), and 1 \times penicillin-streptomycin (Fujifilm). Hepatocytes were seeded in 24-well plates coated with atelocollagen (KOKEN, IPC-30) in basal medium supplemented with 10% FBS at 5×10^4 cells/well and cultured at 37 °C. Three to 4 h after seeding, the medium was replaced with serum-free basal medium. The next day, medium was replaced with basal medium supplemented with DMSO or 20 μM BH_2 and/or 10 μM αT for 1 h at 37 °C. The medium was replaced with the basal medium containing 100 mM HEPES pH 7.4 and DMSO/ $\text{BH}_2/\alpha\text{T}$, and the cells were incubated at 4 °C in refrigerator.

qRT-PCR

cDNA was synthesized from the total RNA of HapT1 cells using the PrimeScript RT Reagent Kit (Takara Bio). The amounts of Pts and Actb were quantified on a LightCycler 480 (Roche) using TB Green Premix ExTaq II (Takara Bio) with the following primers: Pts-F(5'-TACATGGAGGAGGCCAT-CAT-3'), Pts-R(5'-TCTGTTGTGCTTACAACGTC-3'), Actb-F(5'-AAGGCCAACCGT GAAAAGAT-3'), and Actb-R(5'-CCAGAGGCATACAGGGACAG-3').

Statistics and reproducibility

Statistical analyses were conducted using R or GraphPad PRISM. We repeated the same experiments at least three times except for Fig. 1d, which is based on technical triplicate data. Each sample size is indicated in the figure or legend. Any samples or animals were not excluded from the analysis. Randomization and blinding were not used.

RESULTS

Gain-of-function screening identified Gpx4 as a suppressor of cold-induced cell death in human cancer cell lines

At 4 °C, the Syrian hamster pancreatic cancer cell line HapT1 survived 5 days while the human fibroma cell line HT1080 died within 2 days (Fig. 1a). We hypothesized that HapT1 expresses genes that can confer long-term cold resistance not only to hamster cells but also to cold-vulnerable human cells if exogenously introduced. To identify such genes, we conducted expression screening in which a full-length cDNA library prepared from HapT1 cultured at 37 °C was stably introduced and expressed in a cold-vulnerable HT1080 via the piggyBAC transposon system (Fig. 1b). The expression of introduced genes was induced by doxycycline (Dox) under the control of the Tet-ON system. The bulk of the HT1080 cells were exposed to repeated cycles of 4 °C for 6 days and 37 °C for several days, which mimics the situation of deep torpor-arousal cycles. This treatment hardly allowed the survival of the cells without Dox but recovered the cell population in the presence of Dox, implying that the recovered cells acquired resistance to cold-rewarming stress by overexpression of hamster genes integrated into its genome. We then extracted genomic DNA from the surviving cells and analyzed the hamster genes that were stably integrated in the cells (Fig. 1b). As a result, 15 genes were identified, and only Gpx4 was inserted into the genome of surviving cells in three independent screening trials (Fig. 1c). In addition, when each of the 15 hamster genes was independently introduced and exogenously expressed in HT1080, only Gpx4 provided cold-resistance to HT1080 (Fig. 1c, d).

Loss of Gpx4 function abolishes long-term cold resistance in hamster cells due to the accumulation of lipid peroxide

We next addressed whether Gpx4 was required for cold resistance in HapT1 cells. Three independent Gpx4 knockout (KO) HapT1 lines were established using the CRISPR-based VIKING method [30] (Fig. 2a). These Gpx4 KO lines proliferated without obvious abnormalities at 37 °C (data not shown). When exposed to cold (4 °C), most Gpx4 KO cells survived for 2 days, but died by day5 (Fig. 2b). Cell death in Gpx4 KO HapT1 cells induced by prolonged cold stress was prevented by ferroptosis inhibitors, iron chelator (deferrioxamine), lipophilic antioxidant (Ferrostatin-1), and coenzyme Q mimetics (idebenone and mitoquinol) (Fig. 2c). In addition, similar to a previous report on human cells [33], a calcium chelator (BAPTA-AM)

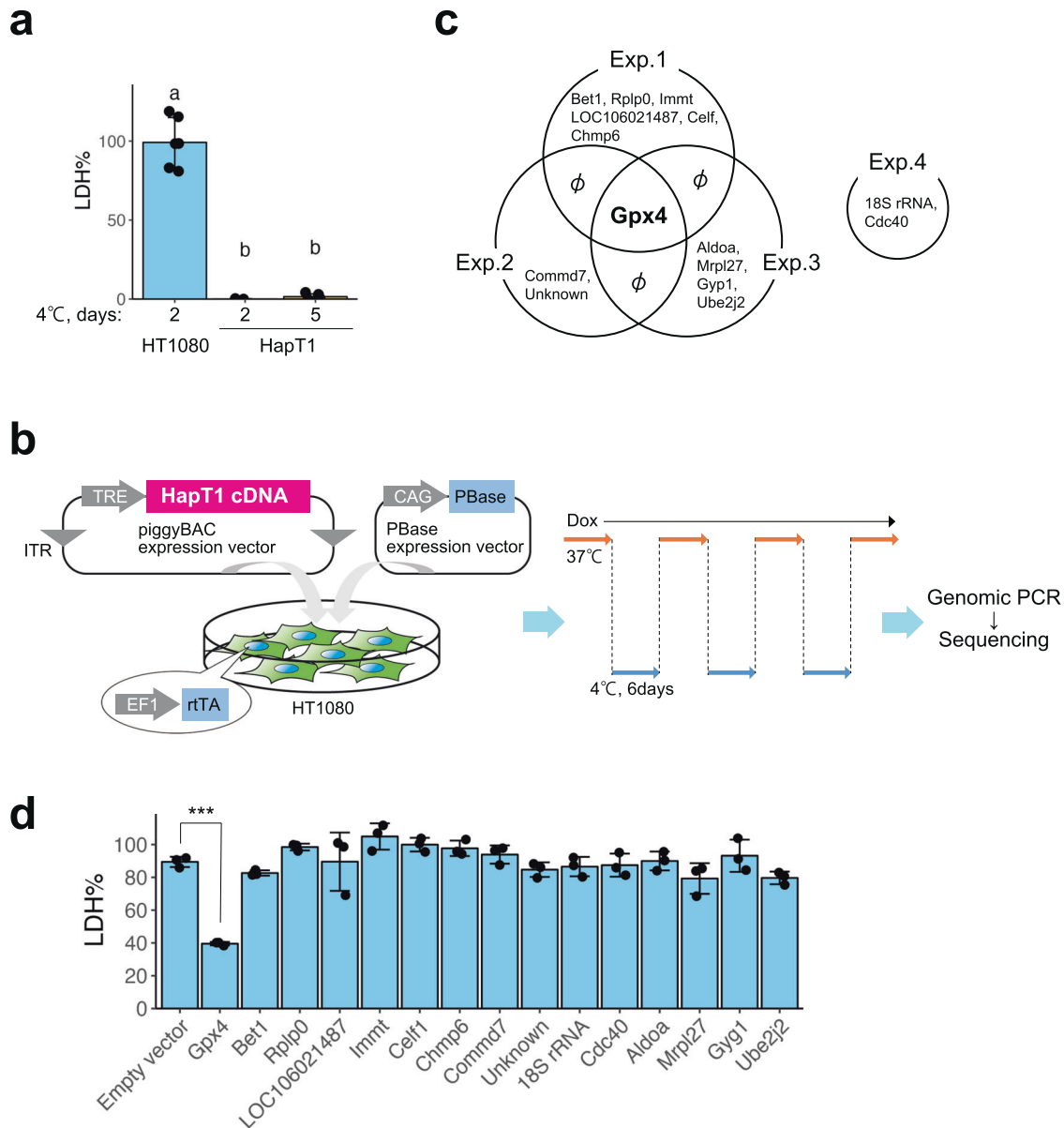
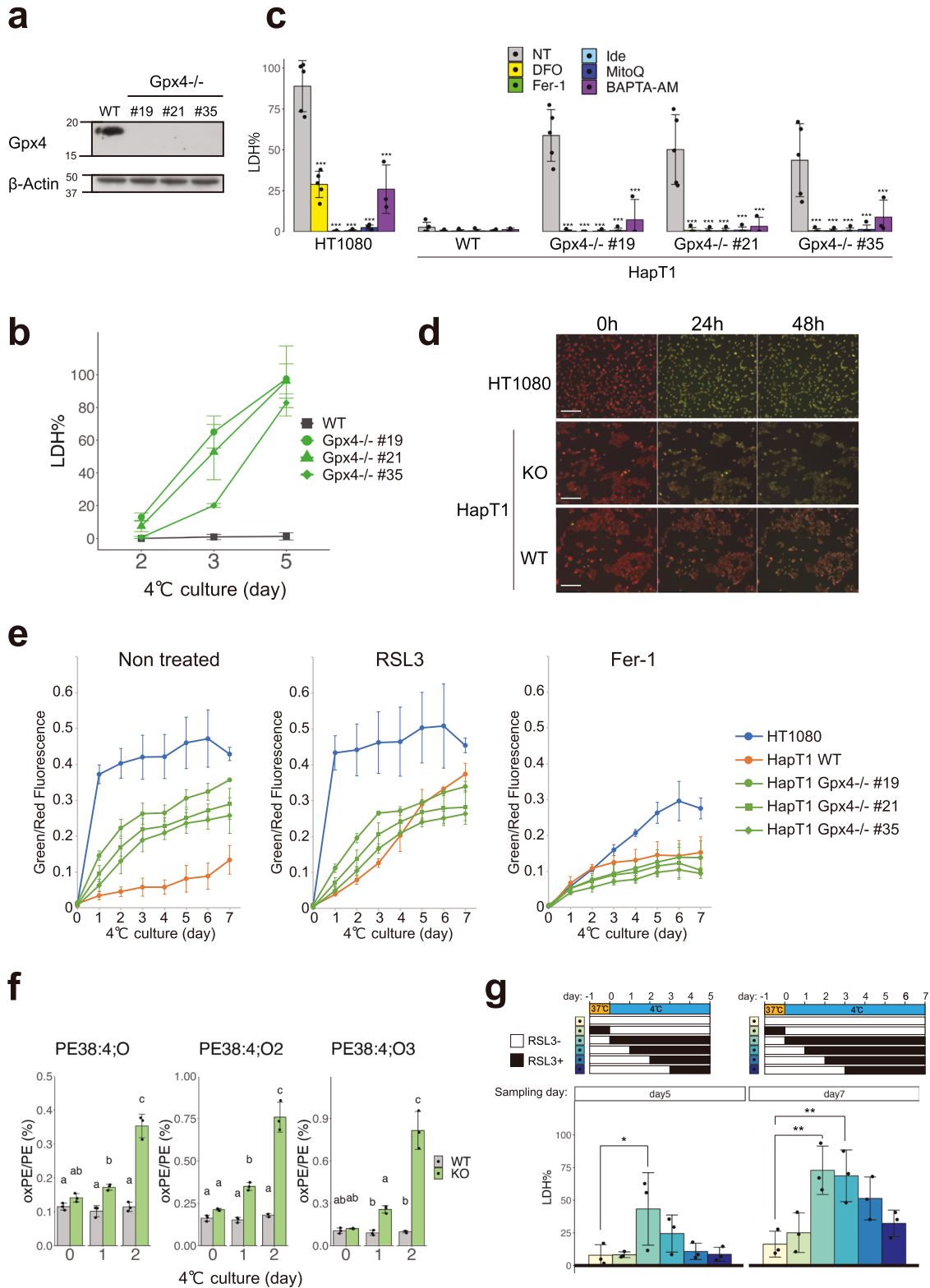


Fig. 1 Gpx4 was identified by hamster cDNA expression screening as a gene rendering cold resistance to a human cancer cell line. **a** Cold resistance of hamster HapT1 cells but not of human HT1080 cells. The proportion of dead cells was determined by LDH assay (one-way ANOVA with the Tukey's multiple comparison test, $p < 0.05$). **b** Schematic illustration of hamster cDNA expression screening for genes that render the resistance to cold-rewarming culture to human HT1080 cells. **c** Venn diagram of the genes inserted in the genome of survived cells under cold-rewarming culture in four screening experiments. **d** The proportion of dead cells in HT1080 cells after 24 h of cold (4 °C) culture when each indicated gene was overexpressed ($N = 3$ wells, One-way ANOVA with the Dunnett's multiple comparison test, $***p < 0.001$).

inhibited cell death of Gpx4 KO HapT1 cells in cold conditions (Fig. 2c, See "Discussion"). We then examined another hallmark of ferroptosis, lipid peroxidation, using live-imaging analysis with BODIPY C11. This analysis revealed that lipid peroxidation in cold culture was much slower in WT HapT1 cells than that in HT1080 cells (Fig. 2d, e). Gpx4 KO HapT1 cells exhibited a much faster accumulation of lipid peroxide than parental (wild type; WT) HapT1 cells, whereas both Gpx4 KO and WT HapT1 cells exhibited very low levels of lipid peroxidation before cold culture (Fig. 2d, e). Extensive lipid peroxidation by cold culture was also observed in WT HapT1 cells treated with a direct Gpx4 inhibitor, RSL3, at a rate comparable to that in Gpx4 KO lines (Fig. 2e). Consistent with this, oxidized lipids, oxidized phosphatidylethanolamines (PE38:4;O, PE38:4;O₂, and PE38:4;O₃), which are ferroptosis signatures [34], increased in Gpx4 KO HapT1 cells after cold treatment (Fig. 2f).

These results suggested that endogenous Gpx4 acts as a suppressor of cold-induced ferroptosis in HapT1 cells. To examine which period of cold culture Gpx4 exerts its function in preventing cold-induced ferroptosis, we treated WT HapT1 cells with RSL3 at different time windows (Fig. 2g) and quantified the amount of cell death. This experiment demonstrated that duration of Gpx4 dysfunction in cold was well correlated with the proportion of dead cells, and that Gpx4 inhibition at 37 °C before cold culture did not affect the cold resistance of the cells. Therefore, the function of Gpx4 is required at 4 °C, but not at 37 °C, to avoid cold-induced cell death. Consistent with this, metabolome analysis under cold and nutrient-deprived condition revealed that reduced glutathione (GSH) did not show a considerable decline until day 5 under cold, while oxidized glutathione (GSSG) displayed a notable rise by day 2 (Fig. S1a). The intracellular levels of high-energy nucleotides, including ATP,



were also maintained until day 5 (Fig. S1b), whereas most of the amino acids, mitochondrial electron carriers (NAD, NADH) and a reducing equivalent (NADPH) were depleted on the first day of transfer to cold and nutrient-deprived culture conditions (Fig. S1c–e). These data suggest that hamster cells can maintain glutathione to supply reduction power to Gpx4 under cold and nutrient-deprived condition during hibernation. Taken together,

these results suggest that Gpx4 functions in cold culture to confer cellular resistance against cold-induced ferroptosis.

Both hamster and human Gpx4 have potential to render cold resistance

The result that exogenous expression of hamster Gpx4 (maGpx4) increased the survival rate of HT1080 under cold conditions raises the

Fig. 2 Gpx4 is necessary for preventing lipid peroxidation and cell death induced by long-term cold exposure in hamster HapT1 cells. **a** Immunoblot of Gpx4 and β -Actin proteins in parental (wild type; WT) and clonal HapT1 cells (#19, #21, #35) in which Gpx4 gene is disrupted. **b** The proportion of dead cells in WT or Gpx4-KO HapT1 cells during cold (4 °C) culture. **c** The proportion of dead cells in HT1080 and parental or Gpx4-KO HapT1 cells after 5 days of cold (4 °C) culture in the absence (non-treated; NT) or presence of 100 μ M DFO, 1 μ M ferrostatin-1 (Fer-1), 10 μ M idebenone (Ide), 10 μ M mitoquinol (MitoQ), 2 μ M BAPTA-AM (One-way ANOVA with the Dunnett's multiple comparison test compared to NT within each cell line, *** p < 0.001). **d** Oxidized lipid detection by BODIPY C11 ratio imaging in HT1080 and HapT1 cells (parental or Gpx4-KO) during cold (4 °C) culture. Scale bar = 200 μ m. **e** Time-course changes of oxidized lipid level determined with BODIPY C11 ratio imaging in the presence or absence of 2 μ M RSL3 or 1 μ M Fer-1 N = 3. Plot is represented as mean \pm s.d. **f** Detection of lipid peroxidation by LC-MS/MS analysis. The amount of mono-(left), di-(middle), tri-(right) oxidized phosphatidylethanolamine (PE38:4) in WT or Gpx4-KO HapT1 cells are shown (One-way ANOVA with the Tukey's multiple comparison test, p < 0.05). **g** The proportion of dead cells in HapT1 after 5 or 7 days of cold (4 °C) culture in the absence or presence of 2 μ M RSL3. Each bar corresponds to the condition shown in the upper panel wherein RSL3 was added only during the period indicated by black during the culture (One-way ANOVA with the Dunnett's multiple comparison test, * p < 0.05, ** p < 0.01).

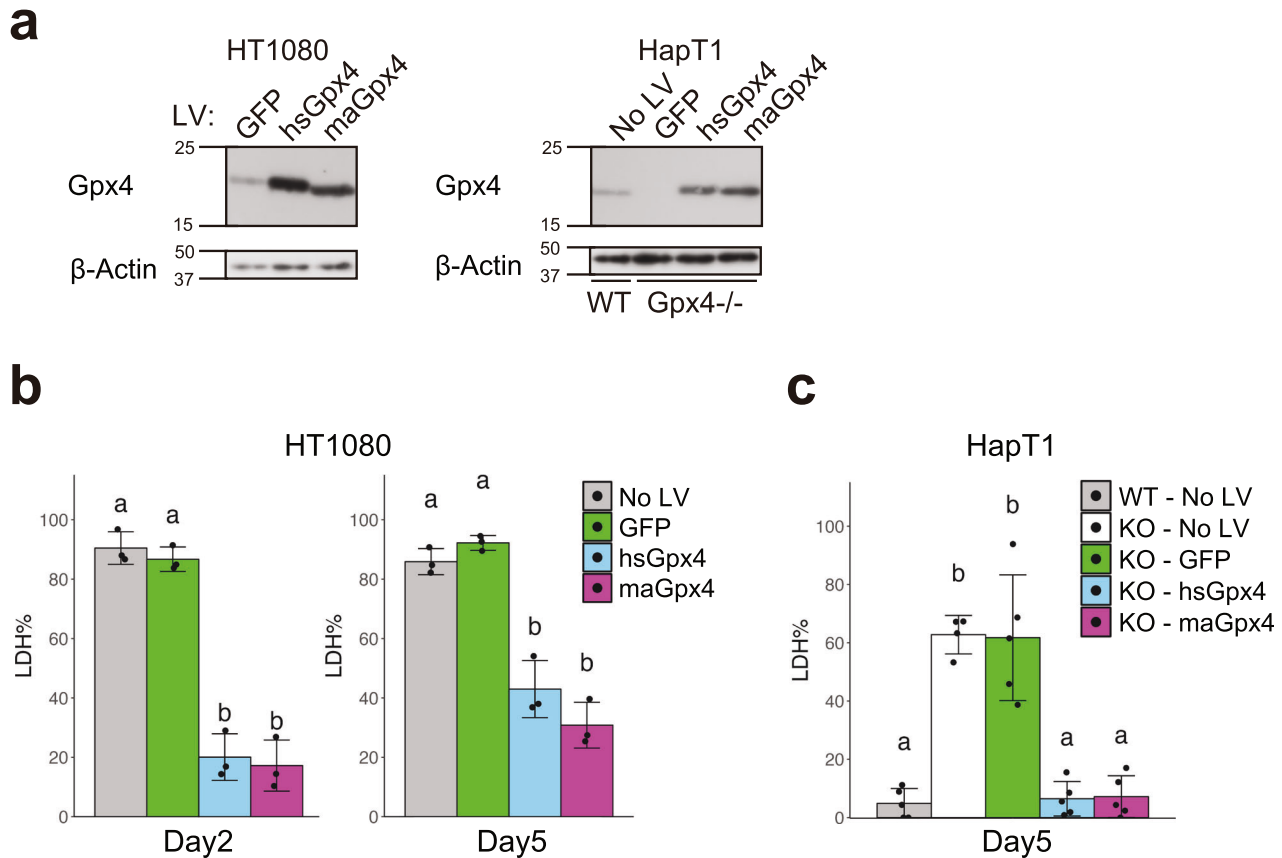


Fig. 3 Overexpression of either human or hamster Gpx4 prevents cold-induced cell death. **a** Immunoblot of Gpx4 and β -Actin proteins in HT1080 and HapT1 (WT and Gpx4-KO clone #21), in which GFP, human (hs)Gpx4, or hamster (ma)Gpx4 were exogenously expressed by lentivirus vectors at 37 °C. The proportion of dead cells after 5 days of cold (4 °C) culture in HT1080 (**b**) and HapT1 (WT or Gpx4-KO) (**c**), in which lentivirus vectors expressing GFP or hs/maGpx4 were infected (One-way ANOVA with the Tukey's multiple comparison test, p < 0.05).

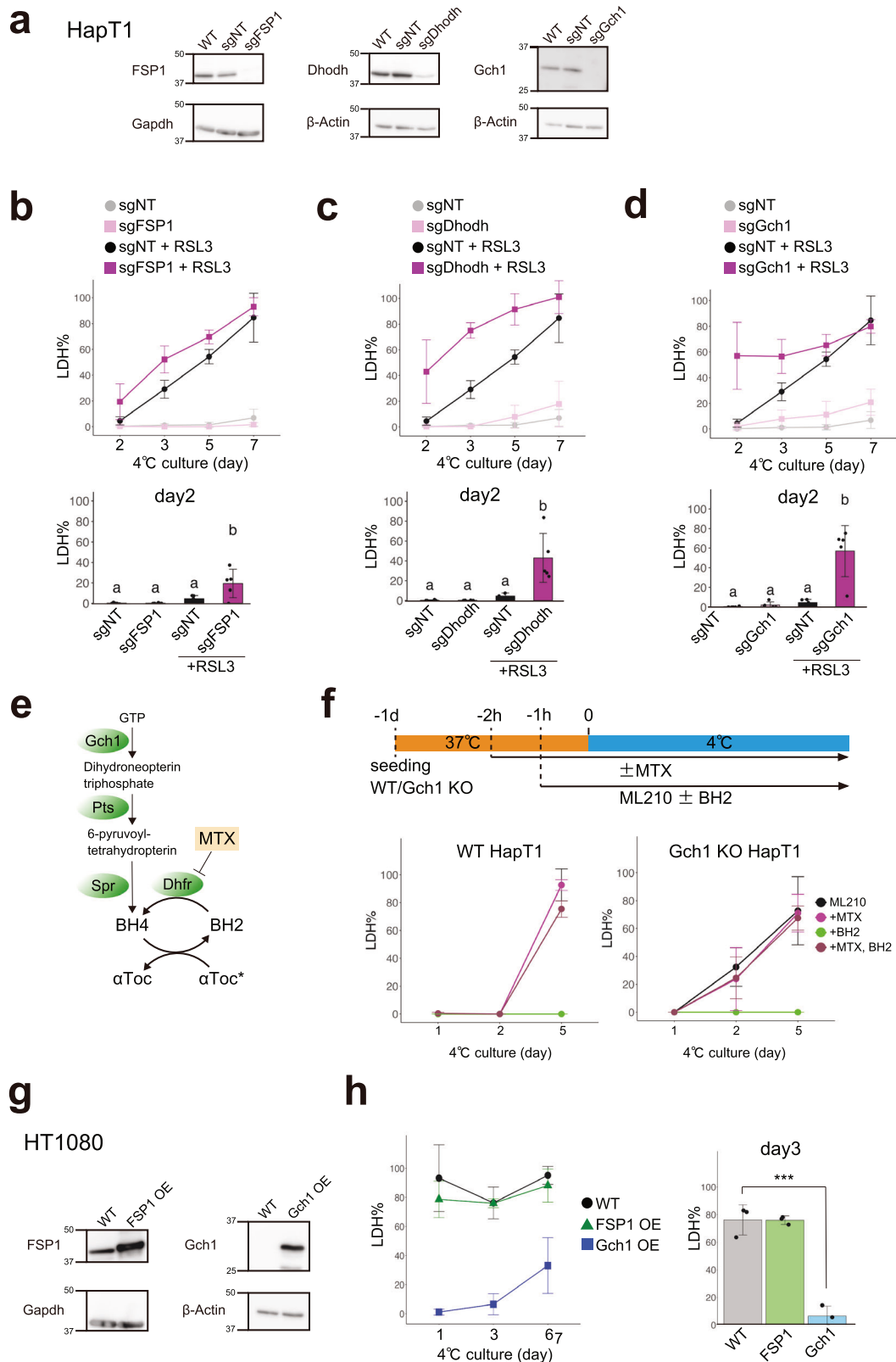
possibility that maGpx4 is more effective in preventing cold-induced ferroptosis than human Gpx4 (hsGpx4), because HT1080 expresses comparable amounts of endogenous hsGpx4 (Figs. 1d and S2a). To test this possibility, we overexpressed either maGpx4 or hsGpx4 in HT1080 cells using lentivirus vectors and examined its effect on cold resistance (Fig. 3a). Overexpression of each Gpx4 gene provided cold resistance to human cells to the same extent (Fig. 3b). In addition, either of these Gpx4 genes restored long-term cold resistance in Gpx4 KO HapT1 cells (Fig. 3a, c). In summary, these results suggest that maGpx4 and hsGpx4 have comparable abilities to prevent cold-induced ferroptosis when overexpressed.

Based on the finding that higher Gpx4 expression provides higher cold resistance in both hibernator and non-hibernator cells, we investigated the expression levels of Gpx4 in the livers of hamsters and mice. The amount of this protein was comparable between the two species (Fig. S2b). Thus, abundance of Gpx4 did

not explain the cold-resistance difference between hamsters and mice. In addition, the protein levels of Gpx4 in both HapT1 and HT1080 did not change after cold treatment (Fig. S2c). Moreover, the expression levels of Gpx4 protein in the hamster liver did not change throughout the seasons (Fig. S2d), excluding the possibility that cold resistance is based on the upregulation of Gpx4 protein level under cold.

Biopterin and CoQ reduction pathways support cold resistance of mammalian cell lines parallel to Gpx4

Although Gpx4 KO HapT1 cells lost long-term cold resistance, they survived for at least two days under cold conditions and therefore can be considered to possess short-term cold resistance (Fig. 2b). To examine whether HapT1 cells possess redundant pathway(s) other than Gpx4 to prevent cold-induced lipid peroxidation and ferroptosis, we knocked out other known ferroptosis suppressors,



namely, FSP1, Dhodh, and Gch1, using the lentiviral CRISPR/Cas9 system (Fig. 4a). A single disruption of each of these genes did not affect the survival rate of HapT1 cells under cold (Fig. 4b–d). However, when treated with Gpx4 inhibitors (RSL3 or ML210), these KO cells died at a significantly higher rate than

WT cells by 2 or 3 days under cold (Figs. 4b–d and S3a–c). These data suggest that each of these genes contributes to cold resistance, in parallel with Gpx4.

Among the three genes, we decided to focus on the Gch1 and bipterin synthesis pathways because Gch1 KO cells exhibited the

Fig. 4 Biopterin and CoQ reduction pathways are required for short-term cold resistance under Gpx4 dysfunction in hamster cells. **a** Assessment of knock-out efficiency of ferroptosis-suppressors in HapT1 cells. Immunoblots of each protein in non-treated HapT1 (WT) or HapT1 cell populations, in which lentivirus vectors expressing SpCas9 and sgRNA (non-targeting control; sgNT, or sgRNA targeting each of three genes) were infected. **b–d** The proportion of dead cells during cold culture (4 °C) in the each HapT1 cell population infected with lentivirus vectors expressing SpCas9 and sgNT or sgRNA for FSP1 (**b**) or Dhodh (**c**) or Gch1 (**d**) in the presence or absence of 2 μ M RSL3 (One-way ANOVA with the Tukey's multiple comparison test, $p < 0.05$). **e** Biopterin synthesis and related pathways. **f** (upper panel) Experimental time course and (lower panel) the proportion of dead cells during cold culture in WT or Gch1 KO HapT1 cells, which were infected with lentivirus vectors expressing SpCas9 and sgNT or sgRNA for Gch1, in the presence of 6 μ M ML210 with or without 100 μ M BH₂ and 4 μ M methotrexate (MTX). **g** Immunoblot of parental HT1080 and HT1080 cell populations in which FSP1 or Gch1 were exogenously overexpressed at 37 °C by lentivirus vector infection. **h** The proportion of dead cells during cold culture in parental HT1080 and HT1080 cell populations in which FSP1 or Gch1 were exogenously overexpressed (One-way ANOVA with the Dunnett's multiple comparison test, *** $p < 0.001$).

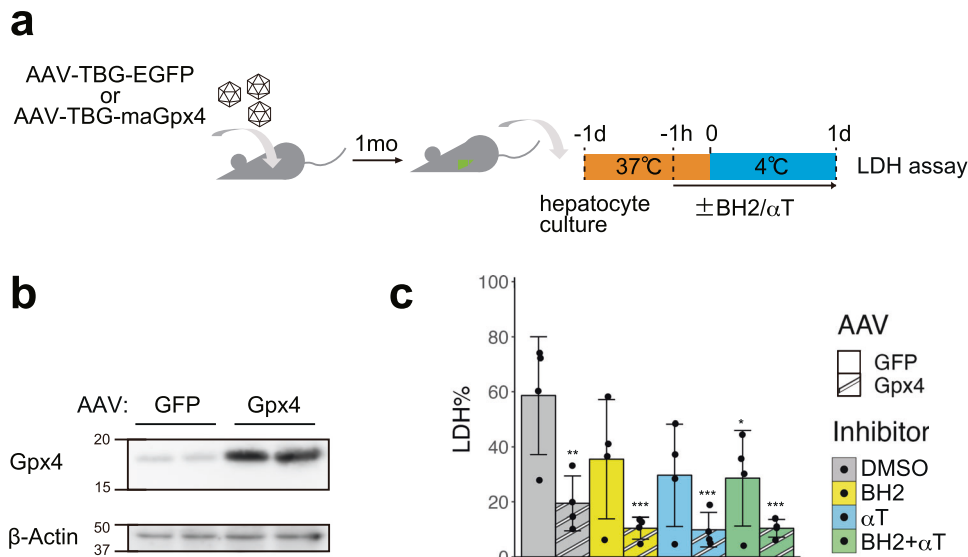


Fig. 5 Gpx4 OE and RTAs additively augment cold resistance of mouse primary hepatocytes. **a** Schematic illustration of experimental time course. **b** Overexpression of Gpx4 protein was confirmed by immunoblot of hepatocytes infected with the AAV vectors expressing GFP or maGpx4. **c** The proportion of dead cells in hepatocytes infected with the AAV vectors expressing GFP or maGpx4 after 24 h cold culture with DMSO or 200 μ M BH₂ and/or 10 μ M α Tocopherol (α T) (one-way ANOVA with the Dunnett's multiple comparison test compared to GFP-DMSO, * $p < 0.05$, ** $p < 0.01$, *** $p < 0.001$).

highest cell death rate on day 2 after treated with Gpx4 inhibitors (Figs. 4d and S3c). Both Pts and Spr encode enzymes that catalyze reactions to form BH₄ downstream of Gch1 in the biopterin synthesis pathway (Fig. 4e). A single KO of Pts or Spr in HapT1 phenocopied that of Gch1 (Fig. S3d–f). Next, we investigated the role of Dhfr, which reduces oxidative biopterin BH₂ to BH₄, in the cold resistance of HapT1. The Dhfr inhibitor methotrexate (MTX) did not affect the survival of HapT1 cells in the absence of Gpx4 inhibitors (Fig. S3g). Dual inhibition of Dhfr and Gpx4 in HapT1 cells did not increase cold-induced cell death compared to Gpx4 inhibition alone (Fig. 4f). These results suggest that the enzymatic activity of Dhfr at 4 °C, if any, does not contribute to the cold resistance of HapT1. On the other hand, supplementation of BH₂ 1 h before cold treatment completely inhibited the cold-induced cell death of both WT and Gch1 KO cells in the presence of a Gpx4 inhibitor ML210, but this effect was abolished by treating the cells with MTX 2 h before cold treatment (Fig. 4f). This suggests that the reduction of exogenous BH₂ to BH₄ by Dhfr at 37 °C before cold treatment is necessary to prevent cold-induced cell death induced by Gpx4 inhibition.

We further addressed whether overexpression of FSP1, Dhodh, or Gch1 could render cold resistance to non-hibernator cells, as well as Gpx4. We infected HT1080 cells with a lentivirus vector that introduced each of these genes derived from hamsters to obtain bulk HT1080 cell lines that overexpressed them (Fig. 4g). Overexpression of Dhodh caused growth defects and did not allow the cell line to be obtained. Overexpression of Gch1 greatly suppressed cold-induced

ferroptosis for 6 days, whereas overexpression of FSP1 did not (Fig. 4h).

Finally, we examined whether these ferroptosis suppressors confer cold resistance to mouse primary hepatocytes (Fig. 5a, b). Mouse hepatocytes overexpressing maGpx4 via AAV infection showed a significantly higher survival rate than the control cells on day1 (Fig. 5c). Moreover, the administration of BH₂ and/or α T with Gpx4 overexpression further augmented the cold resistance of mouse hepatocytes (Fig. 5c). Taken together, BH₄ synthesis and CoQ reduction pathways contribute to the cold resistance of hibernator hamster cells in parallel with Gpx4, and overexpression of Gch1 or biopterin supplementation can suppress cold-induced cell death in non-hibernators such as human and mouse.

DISCUSSION

For improvement of therapeutic hypothermia and better organ preservation under cold temperatures, mammalian hibernation is an ideal nature model of cold resistance. How mammalian hibernators prevent cold-induced cell death, whereas non-hibernators, including humans and mice, are vulnerable to it, is a long-standing and fundamental question. To address this, we used an unbiased screening approach and found that overexpression of Gpx4 confers cold resistance to cold-vulnerable human cell line and mouse primary hepatocytes. This is the first report to empirically demonstrate that Gpx4 is sufficient for rendering cold resistance to non-hibernator human and mouse

cells and is necessary for the intrinsic cold resistance of mammalian hibernator Syrian hamster cells. These findings are plausible considering that cold-induced cell death resembles ferroptosis and that Gpx4 plays pivotal roles in preventing ferroptosis in a wide variety of mammalian tissues and cells, such as the liver [35], kidney [36] and spinal motor neurons [37].

Loss of Gpx4 function in hamster cell lines by genetic or pharmacological methods abolished cold resistance for a long term (5 days) that is approximately the same length as a deep torpor bout of hibernating hamsters at 4 °C ambient temperature. In addition, genetic depletion of Gch1, Dhodh, and FSP1 from HapT1 increased cell death induced by short-term cold treatment under Gpx4 inhibition. These results indicate that biopterin synthesis and plasma membrane/mitochondrial CoQ reduction pathways suppress lipid peroxide accumulation under cold conditions in parallel with Gpx4. Classically, BH₄ is well appreciated as a redox cofactor of several enzymes such as nitric oxide synthase (NOS) and tyrosine hydroxylase (Th), but it has recently been known to affect a wider redox state in cells independently of its role as a cofactor [38, 39]. It has been reported that knockdown of Gch1 in an endothelial cell line led to increased ROS production from mitochondria, largely through a NOS-independent effect [40]. Deficiency of the BH₄ synthesis pathway sensitizes human cell lines to ferroptosis inducers, and an *in vitro* reconstitution assay using liposomes revealed that BH₄ directly or indirectly reduces lipid peroxide radicals via αT [22]. Additionally, in hepatic carcinoma cells, BH₄ suppresses the stress-sensitive Ask1-p38 MAPK signaling pathway [41], which is activated by cold-induced lipid peroxidation in human cell lines [10]. Collectively, we propose that BH₄ contributes to the cold resistance of hibernator cells not as a cofactor of enzymes but as an RTA-reducing lipid peroxide radicals in the membrane. Dhodh is reported to suppress ferroptosis because its inhibition by genetic disruption or administration of BQR at high concentrations (~1 mM) sensitize cells to Gpx4 inhibitor [24]. However, questions regarding the interpretation of these results were raised by the finding that the ferroptosis-promoting effect of high-dose BQR largely relies on FSP1 inhibition but not on Dhodh inhibition and that the effect of Dhodh KO on sensitization to RSL3 is much smaller than that of FSP1 KO [42]. In our case, a single KO of either Dhodh or FSP1 in HapT1 attenuated short-term cold resistance under conditions of Gpx4 dysfunction (Fig. 4b, c), indicating that each of these CoQ-reducing enzymes functions as a suppressor of cold-induced cell death, at least in this hamster cell line.

We propose that the enzymatic activity of Gpx4 at cold temperatures such as 4°C is required to prevent cold-induced cell death based on the following observations: (i) the duration of pharmacological inhibition of Gpx4 in cold is correlated with the proportion of dead cells (Fig. 2g), (ii) inhibition of Gpx4 before cold treatment did not enhance the cell death rate under cold conditions (Fig. 2g), and (iii) Gpx4-KO HapT1 cells accumulated more lipid peroxide than WT cells during cold treatment (Fig. 2d, e). This is in striking contrast to Dhfr, whose activity is required for cell survival by reducing BH₂ to BH₄ before, but not during, cold treatment when Gpx4 does not function (Fig. 4f). Given that enzyme activity generally declines with a decrease in temperature, according to the Arrhenius equation, the enzymatic activity of Gpx4 may be more robust under cold temperatures; that is, it has a lower Q₁₀ value than other general enzymes. Significant enzymatic activity of Gpx4 under cold temperature may be a key to tissue preservation during DT/PA cycles in hibernation because ROS that cause lipid peroxidation and DNA damage increases during cooling without the need of rewarming process in *in vitro* cooling/rewarming experiments [43].

It is unclear why the human Gpx4 protein can prevent cold-induced cell death similar to the hamster protein when its abundance is high (Fig. 3). Among the eight mammalian Gpx family proteins, Gpx4 has the oldest origin [44]. Animal Gpx4 was

derived from a single ancestral protein common to fungi, bacteria, and plants and gave rise to all the other Gpx proteins in the animal kingdom [44]. Therefore, one possible answer to the above question is that the ability of Gpx4 to protect cells from cold-induced ferroptosis may be preserved in poikilothermic organisms for a long history of life and is inherited to present mammals. In addition, transgenic mice overexpressing mitochondrial Gpx4 in the heart maintained cardiac functionality better after ischemia reperfusion (I/R) than WT animals [45]. Accumulating evidence suggests that I/R causes massive ROS production and leads to ferroptosis in thrombosis, such as in stroke and myocardial infarction [46, 47]. Several hibernators exhibit resistance to I/R stress [48, 49], though it has not been elucidated whether cold resistance and I/R resistance share common molecular mechanisms. Hibernators' resistance against I/R stress can be recapitulated by oxygen-glucose deprivation *in vitro* model [50], indicating cell intrinsic mechanisms to prevent I/R-induced ferroptosis. One study reported that under oxygen-deprived conditions, primary renal cells from hamsters expressed Gpx4 at a higher level than those from mice [51]. However, we did not observe any increase in the amount of Gpx4 protein in HapT1 cells after cold exposure (Fig. S2c), and in the livers from animals in very low body temperature at deep torpor compared with others in euthermic periodic arousal or in the non-hibernation period (Fig. S2d). These data suggest that regulation of Gpx4 protein levels is not a mechanism to avoid cold-induced cell death in the hamster cell line and in organs, at least in liver, during hibernation.

It is still an open question why non-hibernator cells are much more vulnerable to cold stress than hibernator cells, even though the expression levels of Gpx4 protein are comparable, as is the case with HT1080 and HapT1 cells (Fig. S2a). As evident from the BODIPY time-course analysis, under cold temperatures, lipid peroxidation occurred far more rapidly in HT1080 than in WT HapT1 or Gpx4-KO HapT1. Thus, HT1080 produced a large amount of lipid peroxides, far beyond the capacity of endogenous Gpx4 for reduction (Fig. 2d, e). As such, in hibernator cells, Gpx4-independent ferroptosis-suppressing pathways, including BH₄- or CoQH₂-mediated pathways, may decrease the production rate of lipid peroxide under cold temperatures to the level at which endogenous Gpx4 can extinguish it. Such a larger capacity of these Gpx4-independent pathways to prevent lipid peroxidation would provide higher cold resistance to hibernators compared to non-hibernators. Another possible explanation is that hibernator cells may have a superior ability to sustain glutathione levels continuously under cold conditions, as suggested in previous studies [9], thereby providing reducing power to Gpx4 and other enzymes that utilize glutathione to combat ROS under cold conditions and to prevent lipid peroxidation (Fig. S1a). Our metabolomic analysis revealed that, unlike most other amino acids, cysteine was maintained and tended to increase under prolonged cold and nutrient-deprived conditions in hamster cells. In addition, the levels of intermediate metabolites involved in glutathione synthesis remained relatively stable (homocysteine and cystathionine). Consistent with this, methionine, the amino acid source for cysteine and glutathione synthesis, was rapidly depleted after cold exposure (Fig. S1a). These data implicate activation of the protein-derived cysteine-cysteine supply pathway, possibly by autophagy, to facilitate the Gpx4-dependent reduction of lipid peroxides.

In normal cellular activity, mitochondria consume most of the O₂ consumed in the cells, and several lines of evidence suggest that mitochondria are one of the important candidates for producing ferroptosis-triggering ROS in cold conditions. At cold temperature, the mitochondria of cells derived from non-hibernators exhibit abnormally high or low membrane potential, whereas those derived from hibernators sustain membrane potential [7, 8]. Genome-wide loss-of-function screening using cold-vulnerable human cancer cell lines revealed that disruption

of MICU1, which positively regulates the transport of Ca^{2+} ions into the mitochondrial matrix, prevents cold-induced cell death [33]. In addition, depletion of intracellular Ca^{2+} by BAPTA-AM in human cancer cells strongly suppressed cold-induced cell death, and this effect was not observed in erastin-induced ferroptosis at 37 °C [33]. These data suggest that unlike drug-induced ferroptosis at 37 °C, cold-induced cell death could be caused by intracellular Ca^{2+} abnormalities leading to mitochondrial dysfunction and ROS production, which eventually oxidizes lipids in the plasma membrane. Considering that Gpx4 and other ferroptosis-suppressors exist in non-hibernators that nevertheless fail to exert cold resistance, it is an interesting topic for future studies to address how hibernators maintain Ca^{2+} homeostasis at cold temperatures.

Collectively, we clarified that hibernator cells can sustain glutathione synthesis pathway under cold conditions and prevent cold-induced ferroptosis through the concerted action of Gpx4-dependent lipid peroxide reduction, biopterin synthesis, and CoQ reduction pathways. We also demonstrated that overexpression of Gpx4 or increasing intracellular BH_4 levels was sufficient to render cold resistance in non-hibernator cells. A limitation of this study is that the contribution of these ferroptosis suppressors to *in vivo* cold resistance during hibernation was not tested. Future studies will address this point through genetic manipulation of these pathways in hamsters using CRISPR/Cas9 or RNAi technologies, which are now feasible for this animal [52, 53]. Other approaches, such as genome-wide loss-of-function screening in hibernator cells, may also help to elucidate crucial components for cold resistance of hibernators other than known ferroptosis-related genes [54]. An additional crucial aspect to consider is the possible oncogenic consequences of altering ferroptosis-associated genes, as they are potential targets of anti-cancer treatments. Hence, it will be necessary to investigate approaches to mitigate any such effects in the context of clinical applications. In conclusion, this study is the first step in addressing the causal relationship of genes and cold resistance of hibernators, one of the long-lasting mysteries of hibernation, thereby providing novel clues for the improvement of clinical applications, such as therapeutic hypothermia and cold preservation for organ transplantation.

DATA AVAILABILITY

The raw data regarding this study are available upon request from the corresponding authors.

REFERENCES

- Geiser F. Hibernation. *Curr Biol* 2013;23:R188–93.
- Ruf T, Geiser F. Daily torpor and hibernation in birds and mammals. *Biol Rev Camb Philos Soc* 2015;90:891–926.
- Geiser F. Hibernation: Endotherms. In: eLS. John Wiley & Sons, Ltd: Chichester; 2011. <https://doi.org/10.1002/9780470015902.a0003215.pub2>.
- Carey HV, Andrews MT, Martin SL. Mammalian hibernation: cellular and molecular responses to depressed metabolism and low temperature. *Physiol Rev* 2003;83:1153–81.
- Anegawa D, Sugiura Y, Matsuoka Y, Sone M, Shichiri M, Otsuka R, et al. Hepatic resistance to cold ferroptosis in a mammalian hibernator Syrian hamster depends on effective storage of diet-derived alpha-tocopherol. *Commun Biol*. 2021;4:796.
- Baudysova M. Cold resistance of cultured cells from hamster and human embryos. *Cryobiology*. 1977;14:506–10.
- Ou J, Ball JM, Luan Y, Zhao T, Miyagishima KJ, Xu Y, et al. iPSCs from a hibernator provide a platform for studying cold adaptation and its potential medical applications. *Cell*. 2018;173:851–63 e16.
- Hendriks KDW, Lupi E, Hardenberg MC, Hoogstra-Berends F, Deelman LE, Henning RH. Differences in mitochondrial function and morphology during cooling and rewarming between hibernator and non-hibernator derived kidney epithelial cells. *Sci Rep*. 2017;7:15482.

- Hendriks KDW, Joschko CP, Hoogstra-Berends F, Heegsma J, Faber KN, Henning RH. Hibernator-derived cells show superior protection and survival in hypothermia compared to non-hibernator cells. *Int J Mol Sci*. 2020;21:1864.
- Hattori K, Ishikawa H, Sakauchi C, Takayanagi S, Naguro I, Ichijo H. Cold stress-induced ferroptosis involves the ASK1-p38 pathway. *EMBO Rep*. 2017;18:2067–78.
- Dixon SJ, Lemberg KM, Lamprecht MR, Skouta R, Zaitsev EM, Gleason CE, et al. Ferroptosis: an iron-dependent form of nonapoptotic cell death. *Cell*. 2012;149:1060–72.
- Jiang X, Stockwell BR, Conrad M. Ferroptosis: mechanisms, biology and role in disease. *Nat Rev Mol Cell Biol*. 2021;22:266–82.
- Conrad M, Pratt DA. The chemical basis of ferroptosis. *Nat Chem Biol*. 2019;15:1137–47.
- Shah R, Farmer LA, Zilka O, Van Kessel ATM, Pratt DA. Beyond DPPH: use of fluorescence-enabled inhibited autoxidation to predict oxidative cell death rescue. *Cell Chem Biol*. 2019;26:1594–607.e7.
- Doll S, Freitas FP, Shah R, Aldrovandi M, da Silva MC, Ingold I, et al. FSP1 is a glutathione-independent ferroptosis suppressor. *Nature*. 2019;575:693–8.
- Bersuker K, Hendricks JM, Li Z, Magtanong L, Ford B, Tang PH, et al. The CoQ oxidoreductase FSP1 acts parallel to GPX4 to inhibit ferroptosis. *Nature*. 2019;575:688–92.
- Savaskan NE, Ufer C, Kuhn H, Borchert A. Molecular biology of glutathione peroxidase 4: from genomic structure to developmental expression and neural function. *Biol Chem*. 2007;388:1007–17.
- Scheerer P, Borchert A, Krauss N, Wessner H, Gerth C, Hohne W, et al. Structural basis for catalytic activity and enzyme polymerization of phospholipid hydroperoxide glutathione peroxidase-4 (GPx4). *Biochemistry*. 2007;46:9041–9.
- Yang WS, SriRamaratnam R, Welsch ME, Shimada K, Skouta R, Viswanathan VS, et al. Regulation of ferroptotic cancer cell death by GPX4. *Cell*. 2014;156:317–31.
- Eaton JK, Furst L, Ruberto RA, Moosmayer D, Hilpmann A, Ryan MJ, et al. Selective covalent targeting of GPX4 using masked nitrile-oxide electrophiles. *Nat Chem Biol*. 2020;16:497–506.
- Yant LJ, Ran Q, Rao L, Van Remmen H, Shibatani T, Belter JG, et al. The selenoprotein GPX4 is essential for mouse development and protects from radiation and oxidative damage insults. *Free Radic Biol Med*. 2003;34:496–502.
- Soula M, Weber RA, Zilka O, Alwaseem H, La K, Yen F, et al. Metabolic determinants of cancer cell sensitivity to canonical ferroptosis inducers. *Nat Chem Biol*. 2020;16:1351–60.
- Kraft VAN, Bezjian CT, Pfeiffer S, Ringelstetter L, Muller C, Zandkarimi F, et al. GTP cyclohydrolase 1/tetrahydrobiopterin counteract ferroptosis through lipid remodeling. *ACS Cent Sci*. 2020;6:41–53.
- Mao C, Liu X, Zhang Y, Lei G, Yan Y, Lee H, et al. DHODH-mediated ferroptosis defense is a targetable vulnerability in cancer. *Nature*. 2021;593:586–90.
- Yoshida A, Yamaguchi Y, Nonomura K, Kawakami K, Takahashi Y, Miura M. Simultaneous expression of different transgenes in neurons and glia by combining *in utero* electroporation with the Tol2 transposon-mediated gene transfer system. *Genes Cells*. 2010;15:501–12.
- Hotta A, Cheung AY, Farra N, Vijayaragavan K, Seguin CA, Draper JS, et al. Isolation of human iPSC cells using EOS lentiviral vectors to select for pluripotency. *Nat Methods*. 2009;6:370–6.
- Naito Y, Hino K, Bono H, Ui-Tei K. CRISPRdirect: software for designing CRISPR/Cas guide RNA with reduced off-target sites. *Bioinformatics*. 2014;31:1120–3.
- Sanjana NE, Shalem O, Zhang F. Improved vectors and genome-wide libraries for CRISPR screening. *Nat Methods*. 2014;11:783–4.
- Panula S, Reda A, Stukenborg JB, Ramathal C, Sukhwani M, Albalushi H, et al. Over expression of NANOS3 and DAZL in human embryonic stem cells. *PLoS ONE*. 2016;11:e0165268.
- Sawatsubashi S, Joko Y, Fukumoto S, Matsumoto T, Sugano SS. Development of versatile non-homologous end joining-based knock-in module for genome editing. *Sci Rep*. 2018;8:593.
- Ruzicka JHA, McHale KJ, Peake DA. Data acquisition parameters optimization of quadrupole orbitrap for global lipidomics on LC-MS/MS time frame. 2014. <https://www.semanticscholar.org/paper/Data-Acquisition-Parameters-Optimization-of-for-Ruzicka-McHale/1c5ed1ce779ebef7012c4be850d868c12506fb4>.
- Konno A, Hirai H. Efficient whole brain transduction by systemic infusion of minimally purified AAV-PHP.eB. *J Neurosci Methods*. 2020;346:108914.
- Nakamura T, Ogawa M, Kojima K, Takayanagi S, Ishihara S, Hattori K, et al. The mitochondrial Ca^{2+} uptake regulator, MICU1, is involved in cold stress-induced ferroptosis. *EMBO Rep*. 2021;22:e51532.
- Kagan VE, Mao G, Qu F, Angeli JP, Doll S, Croix CS, et al. Oxidized arachidonic and adrenic PEs navigate cells to ferroptosis. *Nat Chem Biol*. 2017;13:81–90.
- Carlson BA, Tobe R, Yefremova E, Tsuji PA, Hoffmann VJ, Schweizer U, et al. Glutathione peroxidase 4 and vitamin E cooperatively prevent hepatocellular degeneration. *Redox Biol*. 2016;9:22–31.
- Friedmann Angeli JP, Schneider M, Proneth B, Tyurina YY, Tyurin VA, Hammond VJ, et al. Inactivation of the ferroptosis regulator Gpx4 triggers acute renal failure in mice. *Nat Cell Biol*. 2014;16:1180–91.

37. Chen L, Hambricht WS, Na R, Ran Q. Ablation of the ferroptosis inhibitor glutathione peroxidase 4 in neurons results in rapid motor neuron degeneration and paralysis. *J Biol Chem*. 2015;290:28097–106.
38. Kim HK, Han J. Tetrahydrobiopterin in energy metabolism and metabolic diseases. *Pharm Res*. 2020;157:104827.
39. Eichwald T, da Silva LB, Staats Pires AC, Niero L, Schnorrenberger E, Filho CC, et al. Tetrahydrobiopterin: beyond its traditional role as a cofactor. *Antioxidants*. 2023;12:1037.
40. Bailey J, Shaw A, Fischer R, Ryan BJ, Kessler BM, McCullagh J, et al. A novel role for endothelial tetrahydrobiopterin in mitochondrial redox balance. *Free Radic Biol Med*. 2017;104:214–25.
41. Zhong GC, Zhao ZB, Cheng Y, Wang YB, Qiu C, Mao LH, et al. Epigenetic silencing of GCH1 promotes hepatocellular carcinoma growth by activating superoxide anion-mediated ASK1/p38 signaling via inhibiting tetrahydrobiopterin de novo biosynthesis. *Free Radic Biol Med*. 2021;168:81–94.
42. Mishima E, Nakamura T, Zheng J, Zhang W, Mourao ASD, Sennhenn P, et al. DHODH inhibitors sensitize to ferroptosis by FSP1 inhibition. *Nature*. 2023;619:E9–E18.
43. Tolouee M, Hendriks KDW, Lie FF, Gartzke LP, Goris M, Hoogstra-Berends F, et al. Cooling of cells and organs confers extensive DNA strand breaks through oxidative stress and ATP depletion. *Cell Transplant*. 2022;31:9636897221108705.
44. Trenz TS, Delaix CL, Turchetto-Zolet AC, Zamocky M, Lazzarotto F, Margis-Pinheiro M. Going forward and back: the complex evolutionary history of the GPx. *Biology*. 2021;10:1165.
45. Dabkowski ER, Williamson CL, Hollander JM. Mitochondria-specific transgenic overexpression of phospholipid hydroperoxide glutathione peroxidase (GPx4) attenuates ischemia/reperfusion-associated cardiac dysfunction. *Free Radic Biol Med*. 2008;45:855–65.
46. Lillo-Moya J, Rojas-Sole C, Munoz-Salamanca D, Panieri E, Saso L, Rodrigo R. Targeting ferroptosis against ischemia/reperfusion cardiac injury. *Antioxidants*. 2021;10:667.
47. Yan HF, Tuo QZ, Yin QZ, Lei P. The pathological role of ferroptosis in ischemia/reperfusion-related injury. *Zool Res*. 2020;41:220–30.
48. Otis JP, Pike AC, Torrealba JR, Carey HV. Hibernation reduces cellular damage caused by warm hepatic ischemia-reperfusion in ground squirrels. *J Comp Physiol B*. 2017;187:639–48.
49. Bogren LK, Olson JM, Carpluk J, Moore JM, Drew KL. Resistance to systemic inflammation and multi organ damage after global ischemia/reperfusion in the arctic ground squirrel. *PLoS ONE*. 2014;9:e94225.
50. Bhowmick S, Drew KL. Arctic ground squirrel resist peroxynitrite-mediated cell death in response to oxygen glucose deprivation. *Free Radic Biol Med*. 2017;113:203–11.
51. Eleftheriadis T, Pissas G, Liakopoulos V, Stefanidis I. Factors that may protect the native hibernator Syrian hamster renal tubular epithelial cells from ferroptosis due to warm anoxia-reoxygenation. *Biology*. 2019;8:22.
52. Hirose M, Honda A, Fulka H, Tamura-Nakano M, Matoba S, Tomishima T, et al. Acrosin is essential for sperm penetration through the zona pellucida in hamsters. *Proc Natl Acad Sci USA* 2020;117:2513–8.
53. Dong B, Singh AB, Shende VR, Liu J. Hepatic HNF1 transcription factors control the induction of PCSK9 mediated by rosuvastatin in normolipidemic hamsters. *Int J Mol Med*. 2017;39:749–56.
54. Lam B, Kajderowicz KM, Keys HR, Roessler JM, Frenkel EM, Kirkland A, et al. Multi-species genome-wide CRISPR screens identify GPX4 as a conserved suppressor of cold-induced cell death. *bioRxiv*. 2024. <https://doi.org/10.1101/2024.07.25.605098>.

ACKNOWLEDGEMENTS

We thank Hirotaka Imai (Kitasato University), Jun Suzuki (Kyoto University), Hiroshi Yamaguchi (Nagoya University), Genshiro Sunagawa (Riken BDR), Masayuki Miura (University of Tokyo), and all members of the Yamaguchi Laboratory for their helpful discussions regarding this study.

AUTHOR CONTRIBUTIONS

MS, YS, and YY contributed to the design and implementation of the research, MS, NM, YS, YM, RM, AY, RO, JY, KS, SE, and DA to the performance of experiments and the analysis of the results, MS, YS, and YY to the writing of the manuscript.

FUNDING

This work was supported by the Ministry of Education, Culture, Sports, Science, and Technology (MEXT)/Japan Society for the Promotion of Science KAKENHI (20H05766, 23H28012, 23H04939, 23H04940 to YY, 22K19320, 24K10062 to MS), Japan Agency for Medical Research and Development (AMED) (23gm6310019 to YY), the Grant for Joint Research Program of the Institute of Low Temperature Science, Hokkaido University (19K002), Toray Science Foundation, Takeda Science Foundation, Inamori Research Institute for Science, Cell Science Foundation, Sekisui Chemical Innovations Inspired by Nature Research Support Program, Sumitomo Foundation for Basic Research Projects, Naito Foundation, Uehara Memorial Foundation, Mochida Memorial Foundation for Medical and Pharmaceutical Research, Terumo Life Science Foundation, Joint Research of ExCELLS (No. 21-205 22EXC202) to YY, and Akiyama Life Science Foundation to MS.

COMPETING INTERESTS

The authors declare no competing interests.

ETHICAL APPROVAL AND CONSENT TO PARTICIPATE

All animal care and experimental procedures were approved by the Ethics Committees of Hokkaido University (Ethical Approval no. 18-0140 and 23-0123), and were conducted according to the ethics guidelines of Hokkaido University.

ADDITIONAL INFORMATION

Supplementary information The online version contains supplementary material available at <https://doi.org/10.1038/s41419-024-07059-w>.

Correspondence and requests for materials should be addressed to Masamitsu Sone or Yoshifumi Yamaguchi.

Reprints and permission information is available at <http://www.nature.com/reprints>

Publisher's note Springer Nature remains neutral with regard to jurisdictional claims in published maps and institutional affiliations.



Open Access This article is licensed under a Creative Commons Attribution 4.0 International License, which permits use, sharing, adaptation, distribution and reproduction in any medium or format, as long as you give appropriate credit to the original author(s) and the source, provide a link to the Creative Commons licence, and indicate if changes were made. The images or other third party material in this article are included in the article's Creative Commons licence, unless indicated otherwise in a credit line to the material. If material is not included in the article's Creative Commons licence and your intended use is not permitted by statutory regulation or exceeds the permitted use, you will need to obtain permission directly from the copyright holder. To view a copy of this licence, visit <http://creativecommons.org/licenses/by/4.0/>.

© The Author(s) 2024